Charge imbalanced layered 4*f*-magnet $GdAl_2Ge_2$

Dmitry V. Averyanov, Ivan S. Sokolov, Oleg E. Parfenov, Alexander N. Taldenkov, Oleg A. Kondratev, Andrey M. Tokmachev, Vyacheslav G. Storchak*

National Research Center "Kurchatov Institute", Kurchatov Sq. 1, Moscow 123182, Russia

Abstract

Layered *f*-magnets make a prolific source of unconventional quantum phases and functional properties. Recently, a class of Zintl materials EuA_2X_2 has emerged as holding promise for ideal Weyl and axion physics. The question is whether the magnetic structure, strongly coupled to the topology, can be controlled in such materials *via* a minimal yet selective modification of their chemical composition. Here, we report qualitative changes in the magnetic structure due to charge imbalance. Such imbalance is probed by replacement of Eu with Gd. The two elements form isoelectronic $4f^7$ cations but contribute different numbers of electrons. A synthetic route to epitaxial films of $GdAl_2Ge_2$ on Ge, employing a self-sacrificial template, is proposed. The atomic and magnetic structures of the films, their electron transport properties are studied by a combination of techniques. It is established that the change in the magnetic structure caused by the cationic replacement influences the magnetotransport properties of the films. The results suggest that the charge imbalance in Zintl compounds may provide an instrument to open new routes to functional layered materials with potential applications in spintronics.

Keywords: Zintl phase, valence electron count, $GdAl_2Ge_2$, magnetic anisotropy, magnetotransport

1. Introduction

The variety of available magnetic systems provides a platform for spintronic applications and fundamental studies of quantum effects [1-3]. Special attention is paid to topological [4, 5] and layered [6, 7] magnetic materials; the two research fields often overlap. The interest in layered magnetic materials is spurred by their anisotropic properties and relationship with 2D magnets [8, 9]. Currently, the research is markedly skewed towards *d*-magnets. Yet, layered

* Corresponding author. *E-mail address:* Storchak, V.G. (vgstorchak9@gmail.com)

f-electron materials provide a wealth of magnetic structures [10-12] exhibiting functional properties on par and even exceeding those of layered *d*-magnets. In particular, layered *f*-magnets demonstrate very high [13, 14] and even record-high (among magnetic materials) [15] carrier mobilities. In the 2D limit, rare-earth materials manifest layer-dependent magnetism [16, 17] accompanied by unconventional magnetotransport properties such as colossal negative magnetoresistance (MR) [18]. Thus, rare-earth compounds form an important class of 2D and layered magnets [19]. However, information on structure-property relationships in these systems, central to their functionality, is lacking. A pressing question is how magnetic and transport properties of layered *f*-magnets depend on the chemical composition of the material.

The research on layered *f*-magnets is dominated by Eu-based Zintl compounds. The best studied class of materials is probably EuA_2X_2 of the $CaAl_2Si_2$ structural type (the space group $P\bar{3}m1$) and comprising cationic Eu layers and anionic A_2X_2 bilayers. Most of the 16-electron anions $[A_2X_2]^{2-}$ can be classified according to their elements into 2 types: IIB-VA and IIIA-IVA. The characteristic representatives of the former type are $EuCd_2As_2$ [20-22], $EuCd_2P_2$ [23], $EuCd_2Sb_2$ [24], $EuCd_2Bi_2$ [25], $EuZn_2As_2$ [26, 27], $EuMg_2Bi_2$ [28]. The other type is represented by $EuAl_2Si_2$ [29] and $EuAl_2Ge_2$ [30, 31]; these materials have an advantage of being integrated with semiconductor platforms as epitaxial films [29, 31]. The main rationales behind studies of the EuA_2X_2 compounds are their field tuneable topological structures [20, 22-25, 28] and advantageous magnetotransport properties [21, 22, 29, 31]. In particular, films of $EuAl_2Si_2$ [29] and $EuAl_2Ge_2$ [31] demonstrate high carrier mobility. Surprisingly, replacement of Eu with non-magnetic Sr or Ca results in films [31, 32] and bulk materials [33, 34] with high carrier mobility matching that of the magnetic Eu-based analogues. A possible reason is that conductivity in these charge-balanced Zintl compounds is confined within the anionic layers [35]. One may suppose that deeper changes can be induced by breaking the Zintl structure of the material.

A particularly important outcome of such breaking could be a change of their magnetism. It is well established that the topological structure of the EuA_2X_2 materials depends strongly on their magnetic structure [20, 22, 24, 28, 36-38]. In layered Eu-based materials, the magnetic state is tuneable by modest magnetic fields [20, 21, 28-31, 35, 38] or pressure [39], may depend on the level of band filling [40] or dimensionality [17, 18]. Almost all MA_2X_2 of the $CaAl_2Si_2$ type possess 16 valence electrons [41]. Therefore, unbalancing the Zintl structure to affect the magnetic structure is problematic. For instance, $EuIn_2As_2$, a

candidate axion insulator with unconventional magnetic order [42-44], counts 18 valence electrons but adopts a different atomic structure, preventing direct comparisons. The same applies to $EuSn_2As_2$ counting 20 valence electrons [45]. Cationic replacement seems a more promising route. In particular, Gd and Eu form cations with the same $4f^7$ electronic structure but contribute different numbers of electrons (3 *vs* 2). Typically, such a cation replacement affects the atomic structure: to give an example, anionic layers are stoichiometric and buckled in EuX_2 but non-stoichiometric and flat in GdX_2 [17, 18]. However, the situation with MAl_2X_2 is quite different – both $GdAl_2Si_2$ and $GdAl_2Ge_2$ (17 valence electrons) have been stabilized in the $CaAl_2Si_2$ structure [46, 47]. Their stability is considered an exception to the rule [41, 47]; these charge-imbalanced Zintl phases are characterized as unexpected [46]. The attempts to explain this phenomenon point at the key role of the small electronegativity difference between the atoms of the anionic layer and the lack of a band gap [41, 48]. These Gd-based analogues of $EuAl_2X_2$, whose properties have been studied little so far, thus provide a unique opportunity to answer fundamental questions on the effect of the charge imbalance on the magnetic structure of layered materials.

Here, we study thin films of the charge-imbalanced phase $GdAl_2Ge_2$ setting their properties against those of charge-balanced $EuAl_2Ge_2$. The nanomaterial is synthesized by molecular beam epitaxy employing a sequence of one-dimensional processes based on a self-sacrificial template. The structure of the epitaxial films seamlessly integrated with the semiconducting technological platform of Ge is explored by a combination of diffraction techniques. The magnetic structures of the two compounds are qualitatively different. The resulting transformation of the magnetic structure is demonstrated to have a profound effect on the magnetotransport properties of the materials.

2. Results and discussion

2.1. Synthesis and atomic structure of $GdAl_2Ge_2$ films

Our aim is to produce and study the layered material $GdAl_2Ge_2$. Fig. 1 provides side and top views on the structure of the material, represented by alternating cationic Gd and anionic Al_2Ge_2 layers. The flat Gd layers compose a triangular lattice while the honeycomb anionic slabs are formed by $AlGe_4$ tetrahedra connected to neighbouring tetrahedra by 3 edges. The same structure is adopted by other $REAl_2Ge_2$ systems – $EuAl_2Ge_2$ [31], $HoAl_2Ge_2$ [49], and $DyAl_2Ge_2$ [50]. Synthesis and crystal growth of bulk materials of the $CaAl_2Si_2$ structural type has been studied extensively due to various applications, in particular because many of these

materials exhibit advantageous thermoelectric properties [41]. Different techniques are employed but the common motif is direct synthesis from the elements. Bulk $GdAl_2Ge_2$ has been synthesized by arc melting; a problem of such an approach is the presence of an impurity phase [51]. The situation is particularly difficult if epitaxial films of MA_2X_2 are required. In this case, direct syntheses of MAl_2Si_2 on Si and MAl_2Ge_2 on Ge fail [31, 52] – the resulting films are polycrystalline. The problem is associated with a significant lattice mismatch between the target material and the substrate. Therefore, alternative synthetic routes are necessary.

In synthesis of $GdAl_2Ge_2$, we employ reactive molecular beam epitaxy, a versatile technique allowing for kinetic control over reactions on the monolayer (ML) scale. Certain key aspects of the problem should be taken into consideration. First, the choice of the substrate. We employ germanium wafers for 2 main reasons: Ge provides a technologically important semiconductor platform and it can also serve as one of the reactants. Second, the symmetry match between the material and the substrate is a driver of epitaxy. We are aiming at the layered structure of $GdAl_2Ge_2$ to be parallel to the substrate surface. Therefore, we carry out synthesis on Ge(111) which germanene-like surface has the same three-fold rotation axis as the structure of $GdAl_2Ge_2$. However, lattice match of Ge(111) and $GdAl_2Ge_2$ is far from being perfect: roughly, their corresponding parameters *a* amount to 4.00 Å and 4.25 Å [47, 51]. Synthesis of Ge-based materials can be assisted by reactive precursors [53]. Accordingly, the mismatch problem in epitaxial synthesis of MA_2X_2 is usually solved by an intermediate step – formation of the reactive precursor MX_2 [29, 31, 32, 52]. The current understanding is that this step mitigates the lattice mismatch because $a(X(111)) < a(MX_2) < a(MA_2X_2)$. In synthesis of $GdAl_2Ge_2$, the precursor would be germanene-based $GdGe_2$. However, the lattice parameter *a* of $GdGe_2$ is close to that of Ge(111) [18]. Therefore, it may seem that the $GdGe_2$ precursor is of no use in synthesis of $GdAl_2Ge_2$. This is not the case. Although $GdGe_2$ does not contract the lattice mismatch, it creates the layered scaffold similar to the structure of $GdAl_2Ge_2$. Moreover, the perfect lattice match between Ge(111) and $GdGe_2$ supports the epitaxial character of the films.

The implemented synthesis procedure comprises several steps. First, the Ge(111) surface of the substrate is prepared by removing the natural surface oxide *via* a combination of wet-etching and heating. Then, 4 ML of $GdGe_2$ are formed by deposition of Gd on the heated Ge(111) surface, in accordance with Ref. [18]. Superficially, the reaction corresponds to intercalation of Gd atoms between covalently bound germanene layers of the Ge(111)

surface but it actually proceeds layer-by-layer *via* the vacancy mechanism. Next, $GdGe_2$ is transformed into $GdAl_2Ge_2$ by reaction with Al deposited on top of $GdGe_2$. Therefore, $GdGe_2$ can be considered as a self-sacrificial template. The reaction with Al is likely to proceed layerwise, as demonstrated for another MX_2 compound, $SrSi_2$ [52]: Al atoms reach a germanene layer in $GdGe_2$ and then the reaction propagates along this layer. Although this sequence of steps does result in the required material $GdAl_2Ge_2$, it is not a practical approach to make epitaxial films of substantial thickness. The reason is hindered and uneven access of Al to deep layers of a thick $GdGe_2$ film. Therefore, synthesis of $GdAl_2Ge_2$ films includes an additional step – co-deposition of Al and Gd on top of the ultrathin (4 ML) $GdAl_2Ge_2$ template to produce the bulk of the film. In general terms, the overall synthesis can be characterized as a sequence of one-dimensional topochemical processes [52]. Their details are given in the Experimental section. A series of films of different thickness *d* have been fabricated according to this synthetic route.

It should be noted that the synthesis of the film requires mild conditions, in contrast to that of the bulk [51]. This is important because $GdAl_2Ge_2$ has stability issues: it is mechanically unstable according to calculations of Ref. [54]; annealing at 800 °C destroys this phase [51]. On the other hand, $GdAl_2Ge_2$ may react with the components of air, affecting the material properties. To avoid this chemical degradation, the films are capped by a layer of amorphous insulating SiO_x deposited at room temperature. Such a capping layer does not affect the results of *ex situ* studies of the structure and properties of $GdAl_2Ge_2$.

The structure of the $GdAl_2Ge_2$ films is analysed by a combination of diffraction techniques (Fig. 2). All the synthesis procedures are monitored *in situ* by reflection high-energy electron diffraction (RHEED). The RHEED image of the film (Fig. 2a) confirms its epitaxial character, the $GdAl_2Ge_2$ layers being parallel to the surface; the orientation can be described as $GdAl_2Ge_2[2\bar{1}\bar{1}0] \parallel Ge[1\bar{1}0]$ and $GdAl_2Ge_2[01\bar{1}0] \parallel Ge[11\bar{2}]$, *i.e.* the honeycomb structure of the anionic Al_2Ge_2 layers matches the honeycomb structure of the Ge(111) surface. The distance between the peaks in the 3D RHEED image allows for determination of the lattice parameter *a*; its value 4.26(4) Å agrees with the estimates in bulk $GdAl_2Ge_2$ (4.253(2) Å [44] and 4.248 Å [51]). The structure of the $GdAl_2Ge_2$ films has been studied *ex situ* by X-ray diffraction (XRD) techniques. Fig. 2b demonstrates a typical θ-2θ XRD scan for the material, presenting a set of 7 pronounced reflexes (000*n*). This scan confirms the epitaxial relationship between the $GdAl_2Ge_2$ film and the substrate. It also

signifies the absence of side products in the $GdAl_2Ge_2$ films. The combined fit of the reflex positions determines the lattice parameter *c* of $GdAl_2Ge_2$ to be 6.7083(15) Å, somewhat smaller than the *c* parameter estimates in bulk $GdAl_2Ge_2$ (6.716(2) Å [47] and 6.714 Å [51]). Summarizing, the structural studies certify that the synthesis of epitaxial films of $GdAl_2Ge_2$ on Ge(111) has been successful.

2.2. Magnetism of the films

The films of $GdAl_2Ge_2$ can be compared with those of $EuAl_2Ge_2$ [31], to identify the role of the charge imbalance. The materials have the identical atomic structures, the same Al_2Ge_2 anions, isolelectronic cations. The difference is in the valence electron count (VEC): VEC = 16 for charge-balanced $EuAl_2Ge_2$ and VEC = 17 for $GdAl_2Ge_2$. How this surplus electron affects the systems' properties? The magnetic response is particularly interesting. Both Eu(II) and Gd(III) form cations with the $4f^7$ configurations; the half-filled *f*-shells provide local magnetic moments of spin origin. Fig. 3a demonstrates temperature dependence of the molar magnetic susceptibility in $GdAl_2Ge_2$ for in-plane and out-of-plane magnetic fields. This is a typical behaviour of an antiferromagnet. However, one immediately notices that the temperature dependence in in-plane magnetic field follows that in out-of-plane magnetic field found in $EuAl_2Ge_2$ [31]. Accordingly, the temperature dependence in out-of-plane magnetic field in $GdAl_2Ge_2$ follows that in $EuAl_2Ge_2$ for in-plane magnetic field. Therefore, one may infer that the magnetic moments in $GdAl_2Ge_2$ are directed out-of-plane, in contrast to the in-plane direction of the magnetic moments in $EuAl_2Ge_2$ and other related compounds such as $EuGe_2$ [13]. Surely, the magnetic structure cannot be firmly determined from the $\chi(T)$ dependences (such as those in Fig. 3a); however, we can certainly state that the charge imbalance affects strongly the magnetic anisotropy, resulting in qualitative changes of the magnetic structure.

The parameters of the AFM ordering in the $GdAl_2Ge_2$ films can be compared with those in the bulk [51, 55]. The feature in Fig. 3a corresponding to the Néel temperature (T_N) is located around 22 K, slightly above $T_N \approx 19.7$ K for the bulk [51]. Analysis of χ in the paramagnetic region determines the effective magnetic moment as $m_{eff} = 8.71(6)\ \mu_B$/Gd, close to $m_{eff} = 8.65\ \mu_B$/Gd for the bulk [55] but noticeably higher than that for $EuAl_2Ge_2$ (8.0(1) μ_B/Eu [30]). The contrast in magnetism of $GdAl_2Ge_2$ and $EuAl_2Ge_2$ can be appreciated by comparison of the Weiss constant: 5.2(3) K for $GdAl_2Ge_2$ *vs* -20.1 K for

$EuAl_2Ge_2$ [31]. This qualitative difference points at significantly different magnetic interactions in the two systems.

One of the most important characteristics of the EuA_2X_2 magnetism is transformation of the AFM order into induced ferromagnetism (iFM) in rather moderate magnetic fields [20-22, 28-31]. For instance, this sort of field-induced transformation is responsible for the appearance of the Weyl states in $EuCd_2As_2$ [38]. The magnetic structure of $GdAl_2Ge_2$ also undergoes an AFM-to-iFM transformation. Temperature dependence of the magnetic susceptibility demonstrates a qualitative change in high magnetic field (Fig. 3b). As the magnetic field increases, two effects show up: the drop in χ below T_N disappears and the characteristic feature marking the magnetic transition shifts to lower temperature. This behaviour is similar to that of $EuAl_2Ge_2$. The key difference can be observed in the dependence of the magnetic moment on the out-of-plane magnetic field (Fig. 3c). The expected pattern is a linear $M(H)$ dependence till the saturation occurs, corresponding to full polarization of the magnetic moments. $EuAl_2Ge_2$ follows this pattern but $GdAl_2Ge_2$ does not. The latter exhibits a non-linear behaviour below the characteristic field of about 2 T. In the case of in-plane magnetic fields, the non-linearity in $M(H)$ is less pronounced. The observed non-linearity is associated with the AFM order: it disappears gradually with temperature and the dependence becomes linear around T_N (Fig. 3d). Another detail of Fig. 3c is that $GdAl_2Ge_2$ requires significantly higher fields for the magnetic moment saturation. Although this difference is only quantitative, it highlights yet again the strong relationship between the chemical composition and magnetism of the material.

2.3. Magnetotransport properties

The changes in the magnetic structure can be corroborated by electron transport measurements (Fig. 4 and 5). The AFM transition in $GdAl_2Ge_2$ is detected in the temperature dependence of the resistivity ρ_{xx} which exhibits a maximum. This feature is associated with critical spin fluctuations at T_N. Application of out-of-plane magnetic field has two effects on the $\rho_{xx}(T)$ dependence (Fig. 4a): the feature corresponding to the AFM transition shifts towards lower temperatures and becomes broader. A similar shift is detected in in-plane magnetic fields (Fig. 4b). It suggests that the AFM-to-iFM transformation occurs irrespective of the magnetic field direction. The strong difference between the lateral electron transport in $GdAl_2Ge_2$ and $EuAl_2Ge_2$ is reflected in the MR in out-of-plane magnetic fields. In $EuAl_2Ge_2$, the low-temperature MR is monotonous and positive; $\rho_{xx}(9\ T)/\rho_{xx}(0) \approx 40$ at $T = 2$ K [31]. In

contrast, the MR in $GdAl_2Ge_2$ is small, on the order of 10 % (Fig. 4c). However, the absence of large positive MR makes the contribution of magnetic transformations more pronounced. Two types of sharp maxima appear in the MR: one around 2 T corresponding to the crossover observed in the $M(H)$ curve (Fig. 3c) and the other around 8.5 T corresponding to the transformation into the iFM state. This difference between the MR of $EuAl_2Ge_2$ and $GdAl_2Ge_2$ is again a consequence of the surplus electron in the latter. In charge-balanced $EuAl_2Ge_2$, the electron transport is confined to anionic layers – carriers acquire high mobility resulting in strong positive MR. Apparently, in charge-imbalanced $GdAl_2Ge_2$, the electronic states of the cationic and anionic layers are more coupled, and the MR follows changes in the magnetic structure.

Fig. 4c demonstrates a hysteresis in the MR in out-of-plane magnetic fields. The hysteresis emerges between the two maxima suggesting that this region corresponds to a complex magnetic structure comprising iFM and AFM domains. In contrast, the region below 2 T does not show hysteretic dependence; thus, the crossover is likely to be between AFM and mixed AFM/iFM magnetic systems. A somewhat similar picture is observed for the MR in in-plane magnetic fields orthogonal to the current. In comparison, the negative MR in magnetic fields parallel to the current is not sensitive to the transition into the iFM state; also, the hysteresis is negligibly small. Being sensitive to magnetic transformations, the MR depends on temperature. Fig. 5 shows the evolution of the MR with temperature; a simple negative MR shows up in the paramagnetic phase. As temperature increases, the peak corresponding to the transition into the iFM state shifts to lower magnetic fields. Surprisingly, the crossover at 2 T is rather insensitive to temperature.

The present work provides a coarse-grained description of the changes incurred by charge imbalance in the Zintl phase; it will serve as a foundation for future studies. In particular, both theoretical and experimental microscopic studies (probably of bulk samples rather than thin films) are necessary to resolve the magnetic structure of $GdAl_2Ge_2$. That would be no small feat. On the one hand, the systems are strongly correlated materials – recent theoretical studies of EuX_2 and GdX_2 with triangular cationic lattices [56-58] fail to describe the experimental ground magnetic state. On the other hand, certain conclusions based on experimental results may also be controversial for such systems, as the studies of the popular AFM material $EuCd_2As_2$ demonstrate – 3 different magnetic structures have been proposed [35, 59, 60].

3. Conclusion

Design of materials with various advantageous properties depends on our understanding of the relationships between chemical composition, structure and properties. Here, we addressed the role of the charge imbalance in magnetic and transport properties of Zintl phases. To highlight this factor, we required a pair of very similar materials differing by VEC only. Charge-imbalanced $GdAl_2Ge_2$ (VEC = 17) and charge-balanced $EuAl_2Ge_2$ (VEC = 16) fit the bill: the materials are isostructural with the same anionic layer Al_2Ge_2; their cations are isoelectronic, with the $4f^7$ configuration responsible for magnetic properties. We implemented a synthetic route to epitaxial films of $GdAl_2Ge_2$, to compare their properties with those of $EuAl_2Ge_2$ films [31]. The success of the synthesis opens possibilities in the fabrication of other layered Gd-based materials, such as MAX phases by analogy with Ref. [61] – LnAlSi and LnAlGe materials draw attention due to their topological and magnetic properties [62-64]. From the chemical point of view, it would be interesting to find whether the excess electron in $GdAl_2Ge_2$ affects the chemical properties, similar to the 9-electron electride SrAlSi which reduces hydrogen to form a hydride [65]. Our study of the magnetic properties of $GdAl_2Ge_2$ shows that they are qualitatively different from those of $EuAl_2Ge_2$. The difference can be ascribed to the direction of the magnetic moments. Single-ion anisotropy for the $4f^7$ ions is negligible; therefore, magnetic-dipole interaction and other magnetocrystalline anisotropy energies are supposed to play a critical role. The change in the magnetic structure affects strongly the electron transport properties: for instance, magnetoresistance in the 2 compounds differs by more than 2 orders of magnitude. All in all, the results highlight the ability to influence the magnetic and transport properties of layered materials *via* the charge imbalance and suggest that this instrument deserves a prominent place in the toolbox of materials science.

4. Experimental section

4.1. Synthesis

The films of $GdAl_2Ge_2$ on Ge were synthesized in a Riber Compact system for molecular beam epitaxy. All operations were carried out in ultra-high vacuum ($P < 10^{-10}$ Torr). The substrates were 1 inch × 1 inch Ge(111) wafers with miscut angle below 0.5°. The natural surface oxide GeO_x was removed by wet-etching in 5% NH_3(aq) for 5 min and heating the substrate to 650 °C in vacuo. A thermocouple and a PhotriX ML-AAPX/090 infrared pyrometer operating at a 0.9 μm wavelength were employed to monitor the sample

temperature. 4N Gd and 5N Al for synthesis were supplied from Knudsen cell effusion sources; the pressures of Gd and Al were controlled by a Bayard-Alpert ionization gauge.

The synthesis of $GdAl_2Ge_2$ was carried out in 3 steps. First, a template layer of 4 ML $GdGe_2$ was formed by deposition of Gd ($P_{Gd} = 1 \cdot 10^{-8}$ Torr; the Gd effusion cell was heated to $T_{Gd} = 1210$ °C) on the Ge(111) surface heated to 410 °C (the temperature was held constant during the synthesis). Then, $GdGe_2$ was transformed into $GdAl_2Ge_2$ by deposition of the stoichiometric amount of Al ($P_{Al} = 1.7 \cdot 10^{-8}$ Torr; $T_{Al} = 950$ °C). The bulk of the film was grown by co-deposition of Gd ($P_{Gd} = 1 \cdot 10^{-8}$ Torr; $T_{Gd} = 1210$ °C) and Al ($P_{Al} = 3.2 \cdot 10^{-8}$ Torr; $T_{Al} = 985$ °C). To protect the films from air degradation, they were capped with a 200 nm layer of amorphous insulating SiO_x deposited at room temperature.

4.2. Characterization

The atomic structure of the $GdAl_2Ge_2$ films was probed by 2 techniques. First, the film surface was monitored *in situ* by a RHEED diffractometer equipped with the kSA 400 analytical RHEED system. XRD analysis of the film structure was carried out by a Rigaku SmartLab 9 kW X-ray diffractometer employing the Cu $K_{\alpha 1}$ source (wavelength 1.54056 Å). Magnetic properties of the $GdAl_2Ge_2$ films were determined by an MPMS XL-7 SQUID magnetometer. Square samples with a lateral size 5 mm were mounted in plastic straws and oriented with respect to the external magnetic field (the misalignment does not exceed 2°). The measurements employed the reciprocating sample option. The diamagnetic signal of Ge, determined in a separate experiment, was subtracted. The data for out-of-plane magnetic fields are corrected to take into account the demagnetizing factor. A Lake Shore 9709A Hall effect measurement system was employed to determine electron transport properties of $GdAl_2Ge_2$. Four-contact measurements were carried out on square samples (5 mm × 5 mm) and followed the ASTM Standard F76. The electrical contacts were fabricated by deposition of an Ag-Sn-Ga alloy and attested by I-V characteristic curves.

Acknowledgments

This work is supported by NRC “Kurchatov Institute” and the Russian Science Foundation [grants No. 22-13-00004 (synthesis), No. 19-19-00009 (magnetism studies) and No. 20-79-10028 (electron transport studies)]. D.V.A. acknowledges support from the President’s scholarship (SP 3111.2022.5). The measurements have been carried out using equipment of

the resource centres of electrophysical and laboratory X-ray techniques at NRC “Kurchatov Institute”.

References

[1] S. K. Kim, G. S. D. Beach, K.-J. Lee, T. Ono, T. Rasing and H. Yang, *Ferrimagnetic spintronics*, Nat. Mater. **21**, 24 (2022), doi:10.1038/s41563-021-01139-4.

[2] L. Šmejkal, A. H. MacDonald, J. Sinova, S. Nakatsuji and T. Jungwirth, *Anomalous Hall antiferromagnets*, Nat. Rev. Mater. **7**, 482 (2022), doi:10.1038/s41578-022-00430-3.

[3] Y. Deng, Y. Yu, M. Z. Shi, Z. Guo, Z. Xu, J. Wang, X. H. Chen and Y. Zhang, *Quantum anomalous Hall effect in intrinsic magnetic topological insulator $MnBi_2Te_4$*, Science **367**, 895 (2020), doi:10.1126/science.aax8156.

[4] B. A. Bernevig, C. Felser and H. Beidenkopf, *Progress and prospects in magnetic topological materials*, Nature **603**, 41 (2022), doi:10.1038/s41586-021-04105-x.

[5] Q. L. He, T. L. Hughes, N. P. Armitage, Y. Tokura and K. L. Wang, *Topological spintronics and magnetoelectronics*, Nat. Mater. **21**, 15 (2022), doi:10.1038/s41563-021-01138-5.

[6] H. Li, S. Ruan and Y.-J. Zeng, *Intrinsic van der Waals magnetic materials from bulk to the 2D limit: New frontiers of spintronics*, Adv. Mater. **31**, 1900065 (2019), doi:10.1002/adma.201900065.

[7] H. Kurebayashi, J. H. Garcia, S. Khan, J. Sinova and S. Roche, *Magnetism, symmetry and spin transport in van der Waals layered systems*, Nat. Rev. Phys. **4**, 150 (2022), doi:10.1038/s42254-021-00403-5.

[8] K. F. Mak, J. Shan and D. C. Ralph, *Probing and controlling magnetic states in 2D layered magnetic materials*, Nat. Rev. Phys. **1**, 646 (2019), doi:10.1038/s42254-019-0110-y.

[9] B. Huang, M. A. McGuire, A. F. May, D. Xiao, P. Jarillo-Herrero and X. Xu, *Emergent phenomena and proximity effects in two-dimensional magnets and heterostructures*, Nat. Mater. **19**, 1276 (2020), doi:10.1038/s41563-020-0791-8.

[10] Q. Tao, J. Lu, M. Dahlqvist, A. Mockute, S. Calder, A. Petruhins, R. Meshkian, O. Rivin, D. Potashnikov, E. N. Caspi, H. Shaked, A. Hoser, C. Opagiste, R. M. Galera, R. Salikhov, U. Wiedwald, C. Ritter, A. R. Wildes, B. Johansson, L. Hultman, M. Farle, M. W. Barsoum and J. Rosen, *Atomically layered and ordered rare-earth i-MAX phases: A new class of magnetic quaternary compounds*, Chem. Mater. **31**, 2476 (2019), doi:10.1021/acs.chemmater.8b05298.

[11] P. Chen, W. Han, M. Zhao, J. Su, Z. Li, D. Li, L. Pi, X. Zhou and T. Zhai, *Recent advances in 2D rare-earth materials*, Adv. Funct. Mater. **31**, 2008790 (2021), doi:10.1002/adfm.202008790.

[12] J. Xu, X. Chen, Y. Xu, Y. Du and C. Yan, *Ultrathin 2D rare-earth nanomaterials: Compositions, syntheses, and applications*, Adv. Mater. **32**, 1806461 (2020), doi:10.1002/adma.201806461.

[13] O. E. Parfenov, D. V. Averyanov, A. M. Tokmachev, I. S. Sokolov, I. A. Karateev, A. N. Taldenkov and V. G. Storchak, *High-mobility carriers in germanene derivatives*, Adv. Funct. Mater. **30**, 1910643 (2020), doi:10.1002/adfm.201910643.

[14] H. Masuda, H. Sakai, M. Tokunaga, Y. Yamasaki, A. Miyake, J. Shiogai, S. Nakamura, S. Awaji, A. Tsukazaki, H. Nakao, Y. Murakami, T.-h. Arima, Y. Tokura and S. Ishiwata, *Quantum Hall effect in a bulk antiferromagnet $EuMnBi_2$ with magnetically confined two-dimensional Dirac fermions*, Sci. Adv. **2**, e1501117 (2016), doi:10.1126/sciadv.1501117.

[15] S. Lei, J. Lin, Y. Jia, M. Gray, A. Topp, G. Farahi, S. Klemenz, T. Gao, F. Rodolakis, J. L. McChesney, C. R. Ast, A. Yazdani, K. S. Burch, S. Wu, N. P. Ong and L. M. Schoop, *High*

mobility in a van der Waals layered antiferromagnetic metal, Sci. Adv. **6**, eaay6407 (2020), doi:10.1126/sciadv.aay6407.

[16] A. M. Tokmachev, D. V. Averyanov, O. E. Parfenov, A. N. Taldenkov, I. A. Karateev, I. S. Sokolov, O. A. Kondratev and V. G. Storchak, *Emerging two-dimensional ferromagnetism in silicene materials*, Nat. Commun. **9**, 1672 (2018), doi:10.1038/s41467-018-04012-2.

[17] A. M. Tokmachev, D. V. Averyanov, A. N. Taldenkov, O. E. Parfenov, I. A. Karateev, I. S. Sokolov and V. G. Storchak, *Lanthanide f^7 metalloxenes – a class of intrinsic 2D ferromagnets*, Mater. Horiz. **6**, 1488 (2019), doi:10.1039/C9MH00444K.

[18] O. E. Parfenov, A. M. Tokmachev, D. V. Averyanov, I. A. Karateev, I. S. Sokolov, A. N. Taldenkov and V. G. Storchak, *Layer-controlled laws of electron transport in two-dimensional ferromagnets*, Mater. Today **29**, 20 (2019), doi:10.1016/j.mattod.2019.03.017.

[19] A. V. Papavasileiou, M. Menelaou, K. J. Sarkar, Z. Sofer, L. Polavarapu and S. Mourdikoudis, *Ferromagnetic elements in two-dimensional materials: 2D magnets and beyond*, Adv. Funct. Mater. **34**, 2309046 (2024), doi:10.1002/adfm.202309046.

[20] J. Ma, H. Wang, S. Nie, C. Yi, Y. Xu, H. Li, J. Jandke, W. Wulfhekel, Y. Huang, D. West, P. Richard, A. Chikina, V. N. Strocov, J. Mesot, H. Weng, S. Zhang, Y. Shi, T. Qian, M. Shi and H. Ding, *Emergence of nontrivial low-energy Dirac fermions in antiferromagnetic $EuCd_2As_2$*, Adv. Mater. **32**, 1907565 (2020), doi:10.1002/adma.201907565.

[21] F. Du, L. Yang, Z. Nie, N. Wu, Y. Li, S. Luo, Y. Chen, D. Su, M. Smidman, Y. Shi, C. Cao, F. Steglich, Y. Song and H. Yuan, *Consecutive topological phase transitions and colossal magnetoresistance in a magnetic topological semimetal*, npj Quantum Mater. **7**, 65 (2022), doi:10.1038/s41535-022-00468-0.

[22] S. Roychowdhury, M. Yao, K. Samanta, S. Bae, D. Chen, S. Ju, A. Raghavan, N. Kumar, P. Constantinou, S. N. Guin, N. C. Plumb, M. Romanelli, H. Borrmann, M. G. Vergniory, V. N. Strocov, V. Madhavan, C. Shekhar and C. Felser, *Anomalous Hall conductivity and Nernst effect of the ideal Weyl semimetallic ferromagnet $EuCd_2As_2$*, Adv. Sci. **10**, 2207121 (2023), doi:10.1002/advs.202207121.

[23] E. Heinrich, T. Posske and B. Flebus, *Topological magnetic phase transition in Eu-based A-type antiferromagnets*, Phys. Rev. B **106**, 214402 (2022), doi:10.1103/PhysRevB.106.214402.

[24] H. Su, B. Gong, W. Shi, H. Yang, H. Wang, W. Xia, Z. Yu, P.-J. Guo, J. Wang, L. Ding, L. Xu, X. Li, X. Wang, Z. Zou, N. Yu, Z. Zhu, Y. Chen, Z. Liu, K. Liu, G. Li and Y. Guo, *Magnetic exchange induced Weyl state in a semimetal $EuCd_2Sb_2$*, APL Mater. **8**, 011109 (2020), doi:10.1063/1.5129467.

[25] H. Wang, N. Mao, X. Hu, Y. Dai, B. Huang and C. Niu, *A magnetic topological insulator in two-dimensional $EuCd_2Bi_2$: Giant gap with robust topology against magnetic transitions*, Mater. Horiz. **8**, 956 (2021), doi:10.1039/D0MH01214A.

[26] J. Blawat, M. Marshall, J. Singleton, E. Feng, H. Cao, W. Xie and R. Jin, *Unusual electrical and magnetic properties in layered $EuZn_2As_2$*, Adv. Quantum Technol. **5**, 2200012 (2022), doi:10.1002/qute.202200012.

[27] E. Yi, D. F. Zheng, F. Pan, H. Zhang, B. Wang, B. Chen, D. Wu, H. Liang, Z. X. Mei, H. Wu, S. A. Yang, P. Cheng, M. Wang and B. Shen, *Topological Hall effect driven by short-range magnetic order in $EuZn_2As_2$*, Phys. Rev. B **107**, 035142 (2023), doi:10.1103/PhysRevB.107.035142.

[28] M. Kondo, M. Ochi, R. Kurihara, A. Miyake, Y. Yamasaki, M. Tokunaga, H. Nakao, K. Kuroki, T. Kida, M. Hagiwara, H. Murakawa, N. Hanasaki and H. Sakai, *Field-tunable Weyl points and large anomalous Hall effect in the degenerate magnetic semiconductor $EuMg_2Bi_2$*, Phys. Rev. B **107**, L121112 (2023), doi:10.1103/PhysRevB.107.L121112.

[29] O. E. Parfenov, D. V. Averyanov, I. S. Sokolov, A. N. Taldenkov, I. A. Karateev, A. M. Tokmachev and V. G. Storchak, *High carrier mobility in a layered antiferromagnet integrated with silicon*, ACS Appl. Mater. Interfaces **13**, 41926 (2021), doi:10.1021/acsami.1c13623.

[30] S. Pakhira, A. K. Kundu, F. Islam, M. A. Tanatar, T. Roy, T. Heitmann, T. Yilmaz, E. Vescovo, M. Tsujikawa, M. Shirai, R. Prozorov, D. Vaknin and D. C. Johnston, *Anisotropic magnetism and electronic structure of trigonal $EuAl_2Ge_2$ single crystals*, Phys. Rev. B **107**, 134439 (2023), doi:10.1103/PhysRevB.107.134439.

[31] D. V. Averyanov, I. S. Sokolov, O. E. Parfenov, A. N. Taldenkov, O. A. Kondratev, A. M. Tokmachev and V. G. Storchak, *A class of high-mobility layered nanomaterials by design*, J. Mater. Sci. Technol. **164**, 179 (2023), doi:10.1016/j.jmst.2023.04.059.

[32] D. V. Averyanov, P. Liu, I. S. Sokolov, O. E. Parfenov, I. A. Karateev, D. Di Sante, C. Franchini, A. M. Tokmachev and V. G. Storchak, *Nanoscale synthesis of ionic analogues of bilayer silicene with high carrier mobility*, J. Mater. Chem. C **9**, 8545 (2021), doi:10.1039/D1TC01951A.

[33] H. Su, X. Shi, W. Xia, H. Wang, X. Hanli, Z. Yu, X. Wang, Z. Zou, N. Yu, W. Zhao, G. Xu and Y. Guo, *Magnetotransport and ab initio calculation studies on the layered semimetal $CaAl_2Si_2$ hosting multiple nontrivial topological states*, Phys. Rev. B **101**, 205138 (2020), doi:10.1103/PhysRevB.101.205138.

[34] S. Malick, A. B. Sarkar, A. Laha, M. Anas, V. K. Malik, A. Agarwal, Z. Hossain and J. Nayak, *Large nonsaturating magnetoresistance, weak anti-localization, and non-trivial topological states in $SrAl_2Si_2$*, Phys. Rev. B **106**, 075105 (2022), doi:10.1103/PhysRevB.106.075105.

[35] M. C. Rahn, J.-R. Soh, S. Francoual, L. S. I. Veiga, J. Strempfer, J. Mardegan, D. Y. Yan, Y. F. Guo, Y. G. Shi and A. T. Boothroyd, *Coupling of magnetic order and charge transport in the candidate Dirac semimetal $EuCd_2As_2$*, Phys. Rev. B **97**, 214422 (2018), doi:10.1103/PhysRevB.97.214422.

[36] J.-Z. Ma, S. M. Nie, C. J. Yi, J. Jandke, T. Shang, M. Y. Yao, M. Naamneh, L. Q. Yan, Y. Sun, A. Chikina, V. N. Strocov, M. Medarde, M. Song, Y.-M. Xiong, G. Xu, W. Wulfhekel, J. Mesot, M. Reticcioli, C. Franchini, C. Mudry, M. Müller, Y. G. Shi, T. Qian, H. Ding and M. Shi, *Spin fluctuation induced Weyl semimetal state in the paramagnetic phase of $EuCd_2As_2$*, Sci. Adv. **5**, eaaw4718 (2019), doi:10.1126/sciadv.aaw4718.

[37] G. Hua, S. Nie, Z. Song, R. Yu, G. Xu and K. Yao, *Dirac semimetal in type-IV magnetic space groups*, Phys. Rev. B **98**, 201116(R) (2018), doi:10.1103/PhysRevB.98.201116.

[38] J.-R. Soh, F. de Juan, M. G. Vergniory, N. B. M. Schröter, M. C. Rahn, D. Y. Yan, J. Jiang, M. Bristow, P. Reiss, J. N. Blandy, Y. F. Guo, Y. G. Shi, T. K. Kim, A. McCollam, S. H. Simon, Y. Chen, A. I. Coldea and A. T. Boothroyd, *Ideal Weyl semimetal induced by magnetic exchange*, Phys. Rev. B **100**, 201102(R) (2019), doi:10.1103/PhysRevB.100.201102.

[39] E. Gati, S. L. Bud'ko, L.-L. Wang, A. Valadkhani, R. Gupta, B. Kuthanazhi, L. Xiang, J. M. Wilde, A. Sapkota, Z. Guguchia, R. Khasanov, R. Valentí and P. C. Canfield, *Pressure-induced ferromagnetism in the topological semimetal $EuCd_2As_2$*, Phys. Rev. B **104**, 155124 (2021), doi:10.1103/PhysRevB.104.155124.

[40] N. H. Jo, B. Kuthanazhi, Y. Wu, E. Timmons, T.-H. Kim, L. Zhou, L.-L. Wang, B. G. Ueland, A. Palasyuk, D. H. Ryan, R. J. McQueeney, K. Lee, B. Schrunk, A. A. Burkov, R. Prozorov, S. L. Bud'ko, A. Kaminski and P. C. Canfield, *Manipulating magnetism in the topological semimetal $EuCd_2As_2$*, Phys. Rev. B **101**, 140402(R) (2020), doi:10.1103/PhysRevB.101.140402.

[41] W. Peng, S. Chanakian and A. Zevalkink, *Crystal chemistry and thermoelectric transport of layered AM_2X_2 compounds*, Inorg. Chem. Front. **5**, 1744 (2018), doi:10.1039/C7QI00813A.

[42] Y. Xu, Z. Song, Z. Wang, H. Weng and X. Dai, *Higher-order topology of the axion insulator $EuIn_2As_2$*, Phys. Rev. Lett. **122**, 256402 (2019), doi:10.1103/PhysRevLett.122.256402.

[43] Y. Zhang, K. Deng, X. Zhang, M. Wang, Y. Wang, C. Liu, J.-W. Mei, S. Kumar, E. F. Schwier, K. Shimada, C. Chen and B. Shen, *In-plane antiferromagnetic moments and magnetic polaron in the axion topological insulator candidate $EuIn_2As_2$*, Phys. Rev. B *101*, 205126 (2020), doi:10.1103/PhysRevB.101.205126.

[44] J.-R. Soh, A. Bombardi, F. Mila, M. C. Rahn, D. Prabhakaran, S. Francoual, H. M. Rønnow and A. T. Boothroyd, *Understanding unconventional magnetic order in a candidate axion insulator by resonant elastic X-ray scattering*, Nat. Commun. **14**, 3387 (2023), doi:10.1038/s41467-023-39138-5.

[45] H. Li, S.-Y. Gao, S.-F. Duan, Y.-F. Xu, K.-J. Zhu, S.-J. Tian, J.-C. Gao, W.-H. Fan, Z.-C. Rao, J.-R. Huang, J.-J. Li, D.-Y. Yan, Z.-T. Liu, W.-L. Liu, Y.-B. Huang, Y.L. Li, Y. Liu, G.-B. Zhang, P. Zhang, T. Kondo, S. Shin, H.-C. Lei, Y.-G. Shi, W.-T. Zhang, H.-M. Weng, T. Qian and H. Ding, *Dirac surface states in intrinsic magnetic topological insulators $EuSn_2As_2$ and $MnBi_{2n}Te_{3n+1}$*, Phys. Rev. X **9**, 041039 (2019), doi:10.1103/PhysRevX.9.041039.

[46] R. Nesper, H. G. von Schnering and J. Curda, *$GdAl_2Si_2$, eine unerwartete Verbindung in $CaAl_2Si_2$-Typ*, Z. Naturforsch. B **37**, 1514 (1982), doi:10.1515/znb-1982-1205.

[47] C. Kranenberg, D. Johrendt and A. Mewis, *The stability range of the $CaAl_2Si_2$-type structure in case of $LnAl_2Ge_2$ compounds*, Solid State Sci. **4**, 261 (2002), doi:10.1016/S1293-2558(01)01237-7.

[48] C. Kranenberg, D. Johrendt and A. Mewis, *Untersuchungen zum Existenzgebiet des $CaAl_2Si_2$-Strukturtyps bei ternären Siliciden*, Z. Anorg. Allg. Chem. 625 1787 (1999), doi:10.1002/(SICI)1521-3749(199911)625:11<1787::AID-ZAAC1787>3.0.CO;2-H.

[49] F. Gao, J. Sheng, W. Ren, Q. Zhang, X. Luo, J. Qi, M. Cong, B. Li, L. Wu and Z. Zhang, *Incommensurate spin density wave and magnetocaloric effect in the metallic triangular lattice $HoAl_2Ge_2$*, Phys. Rev. B **106**, 134426 (2022), doi:10.1103/PhysRevB.106.134426.

[50] F. Gao, W. Ren, H. Wu, M. An, X. Zhao, B. Li and Z. Zhang, *Magnetic properties and magnetocaloric effect of a metallic triangular lattice antiferromagnetic $DyAl_2Ge_2$ single crystal*, J. Solid State Chem. **328**, 124347 (2023), doi:10.1016/j.jssc.2023.124347.

[51] F. M. Mulder, R. C. Thiel and K. H. J. Buschow, *^{155}Gd Mössbauer spectroscopy and magnetic properties of $GdAl_2Ge_2$*, J. Alloys Compd. **226**, 100 (1995), doi:10.1016/0925-8388(95)01590-6.

[52] A. M. Tokmachev, D. V. Averyanov, I. A. Karateev, I. S. Sokolov, O. E. Parfenov and V. G. Storchak, *Dimensionality concept in solid-state reactions: A way to control synthesis of functional materials at the nanoscale*, Adv. Funct. Mater. **30**, 2002691 (2020), doi:10.1002/adfm.202002691.

[53] M. Beekman, S. M. Kauzlarich, L. Doherty and G. S. Nolas, *Zintl phases as reactive precursors for synthesis of novel silicon and germanium-based materials*, Materials **12**, 1139 (2019), doi:10.3390/ma12071139.

[54] H. Wang, Y. Zhan, M. Pang and Y. Du, *Properties of hexagonal Al_2Ge_2RE (RE = Y, La, Ce, Nd, Eu, Gd, Tb, Yb and Lu): A first-principles study*, Solid State Commun. **151**, 1814 (2011), doi:10.1016/j.ssc.2011.08.019.

[55] F. M. Mulder, R. C. Thiel, L. D. Tung, J. J. M. Franse and K. H. J. Buschow, *^{155}Gd Mössbauer spectroscopy and magnetic properties of several ternary Gd compounds*, J. Alloys Compd. **264**, 43 (1998), doi:10.1016/S0925-8388(97)00201-6.

[56] G. Yang, J.-S. Chai, K. Bu, L.-F. Xu and J.-T. Wang, *Structural, magnetic, and electronic properties of $EuSi_2$ thin films on the Si(111) surface*, Phys. Chem. Chem. Phys. **24**, 6782 (2022), doi:10.1039/D1CP05913K.

[57] Z. Gao, Y. Wang, J. Gao, Z. Cui, X. Zhang, J. Shi and X. Fan, *Bipolar ferromagnetic semiconductor with large magnetic moment: $EuGe_2$ monolayer*, Comp. Mater. Sci. **213**, 111611 (2022), doi:10.1016/j.commatsci.2022.111611.

[58] Y. Wang, Z. Cui, H. Zeng, Z. Wang, X. Zhang, J. Shi, T. Cao and X. Fan, *Tunable magnetic order in two-dimensional layered $GdGe_2$*, J. Mater. Chem. C **10**, 1259 (2022), doi:10.1039/D1TC05350G.

[59] H. P. Wang, D. S. Wu, Y. G. Shi and N. L. Wang, *Anisotropic transport and optical spectroscopy study on antiferromagnetic triangular lattice $EuCd_2As_2$: An interplay between magnetism and charge transport properties*, Phys. Rev. B **94**, 045112 (2016), doi:10.1103/PhysRevB.94.045112.

[60] K. M. Taddei, L. Yin, L. D. Sanjeeva, Y. Li, J. Xing, C. dela Cruz, D. Phelan, A. S. Sefat and D. S. Parker, *Single pair of Weyl nodes in the spin-canted structure of $EuCd_2As_2$*, Phys. Rev. B **105**, L140401 (2022), doi:10.1103/PhysRevB.105.L140401.

[61] D. V. Averyanov, I. S. Sokolov, O. E. Parfenov, A. N. Taldenkov, I. A. Karateev, O. A. Kondratev, A. M. Tokmachev and V. G. Storchak, *Thickness-dependent superconductivity in a layered electride on silicon*, Small **19**, 2302065 (2023), doi:10.1002/smll.202302065.

[62] J. Gaudet, H.-Y. Yang, S. Baidya, B. Lu, G. Xu, Y. Zhao, J. A. Rodriguez-Rivera, C. M. Hoffmann, D. E. Graf, D. H. Torchinsky, P. Nikolić, D. Vanderbilt, F. Tafti and C. L. Broholm, *Weyl-mediated helical magnetism in NdAlSi*, Nat. Mater. **20**, 1650 (2021), doi:10.1038/s41563-021-01062-8.

[63] P. Puphal, V. Pomjakushin, N. Kanazawa, V. Ukleev, D. J. Gawryluk, J. Ma, M. Naamneh, N. C. Plumb, L. Keller, R. Cubitt, E. Pomjakushina and J. S. White, *Topological magnetic phase in the candidate Weyl semimetal CeAlGe*, Phys. Rev. Lett. **124**, 017202 (2020), doi:10.1103/PhysRevLett.124.017202.

[64] X. Yao, J. Gaudet, R. Verma, D. E. Graf, H.-Y. Yang, F. Bahrami, R. Zhang, A. A. Aczel, S. Subedi, D. H. Torchinsky, J. Sun, A. Bansil, S.-M. Huang, B. Singh, P. Blaha, P. Nikolić and F. Tafti, *Large topological Hall effect and spiral magnetic order in the Weyl semimetal SmAlSi*, Phys. Rev. X **13**, 011035 (2023), doi:10.1103/PhysRevX.13.011035.

[65] T. Björling, D. Noréus, K. Jansson, M. Andersson, E. Leonova, M. Edén, U. Hålenius and U. Häussermann, *SrAlSiH: A polyanionic semiconductor hydride*, Angew. Chem. Int. Ed. **44**, 7269 (2005), doi:10.1002/ange.200502090.

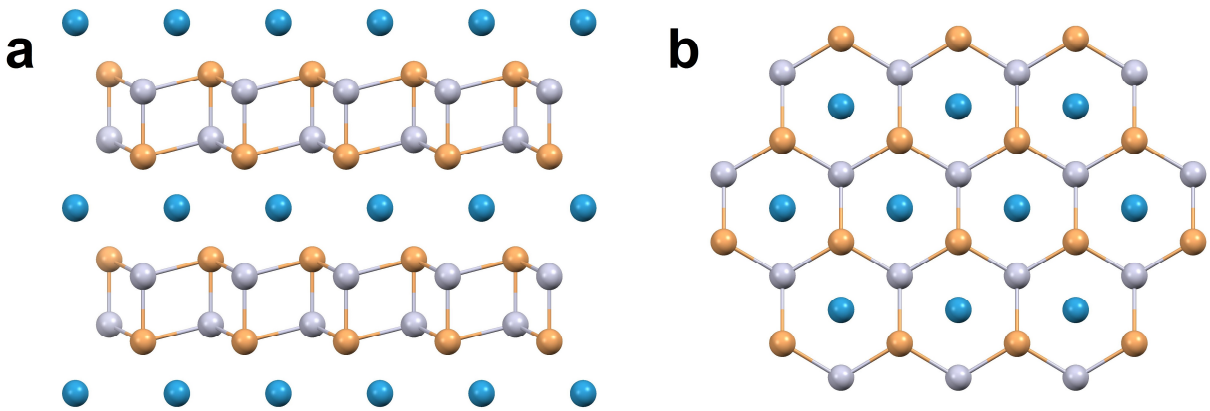

Fig. 1. Ball-and-stick structural model of $GdAl_2Ge_2$ (Gd – blue, Al – grey, and Ge – dark orange). a) Side view demonstrating the layered structure formed by flat cationic layers of Gd and anionic bilayers Al_2Ge_2. b) Top view demonstrating the honeycomb structure.

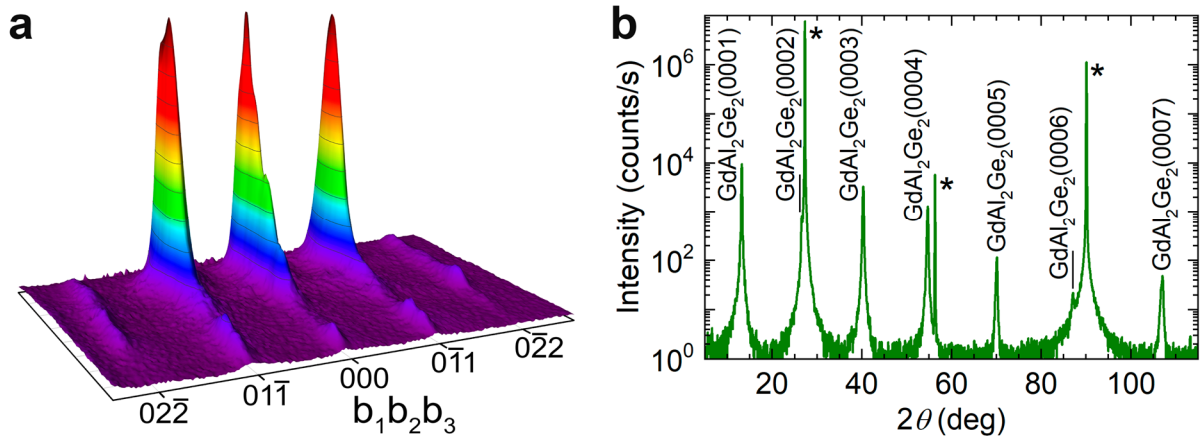

Fig. 2. Structural characterization of $GdAl_2Ge_2$ films on Ge (typical images for d = 38 nm). a) A 3D RHEED image; the reflexes are marked by Miller-Bravais indices for the basal plane ($b_1b_2b_3$). b) A θ-2θ XRD scan; asterisks denote peaks from the Ge(111) substrate.

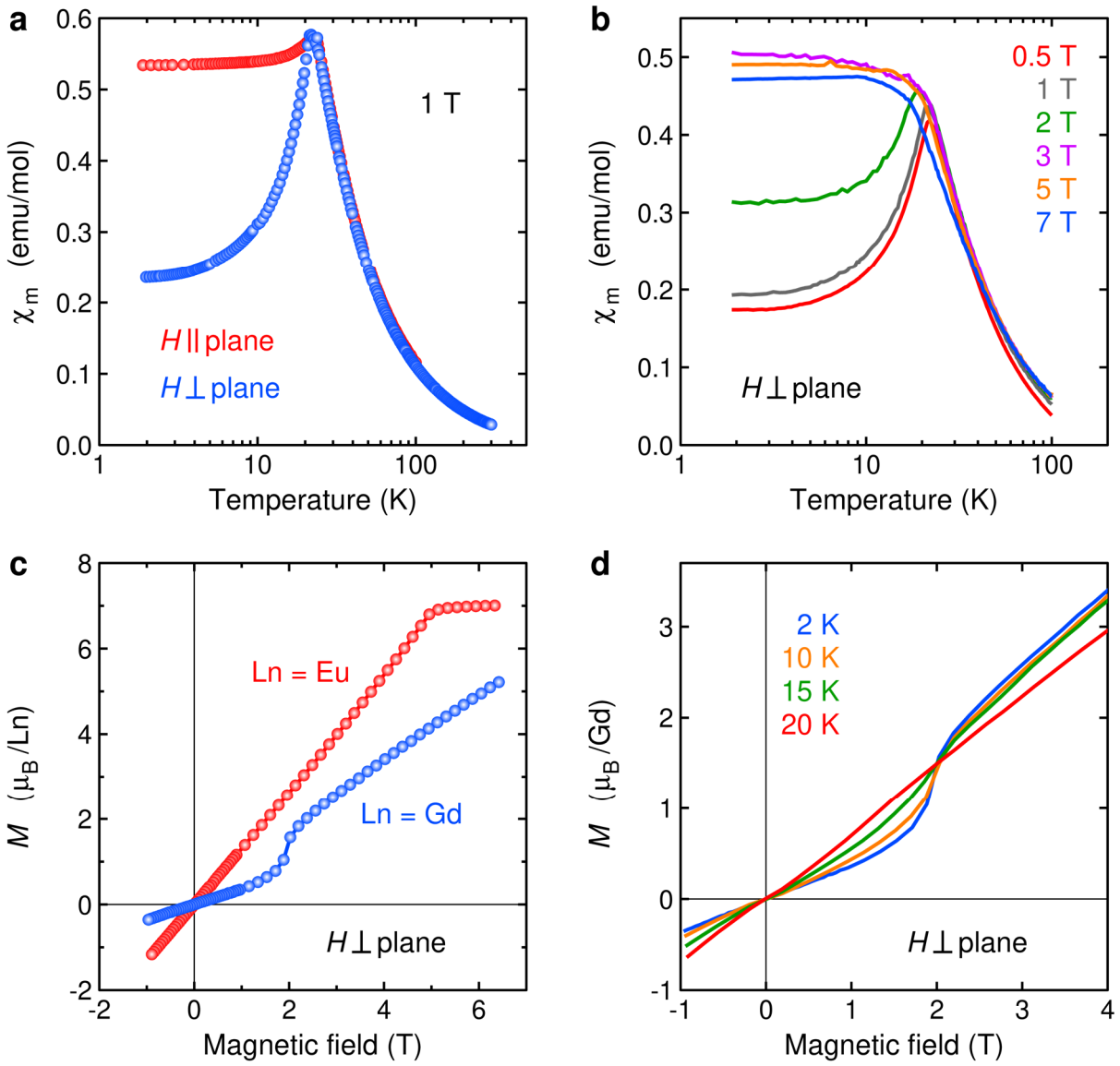

Fig. 3. Magnetic properties of $GdAl_2Ge_2$ films. a) Temperature dependence of the molar magnetic susceptibility of the 115-nm film in in-plane (red) and out-of-plane (blue) magnetic fields 1 T. b) Temperature dependence of the molar magnetic susceptibility of the 38-nm film in out-of-plane magnetic fields 0.5 T (red), 1 T (grey), 2 T (green), 3 T (magenta), 5 T (orange), and 7 T (blue). c) Dependence of the magnetic moment in $GdAl_2Ge_2$ (d = 38 nm) on the out-of-plane magnetic field at 2 K (blue) as compared to the same dependence for $EuAl_2Ge_2$ from Ref. [31]. d) Dependence of the magnetic moment in $GdAl_2Ge_2$ (d = 38 nm) on the out-of-plane magnetic field at 2 K (blue), 10 K (orange), 15 K (green), and 20 K (red).

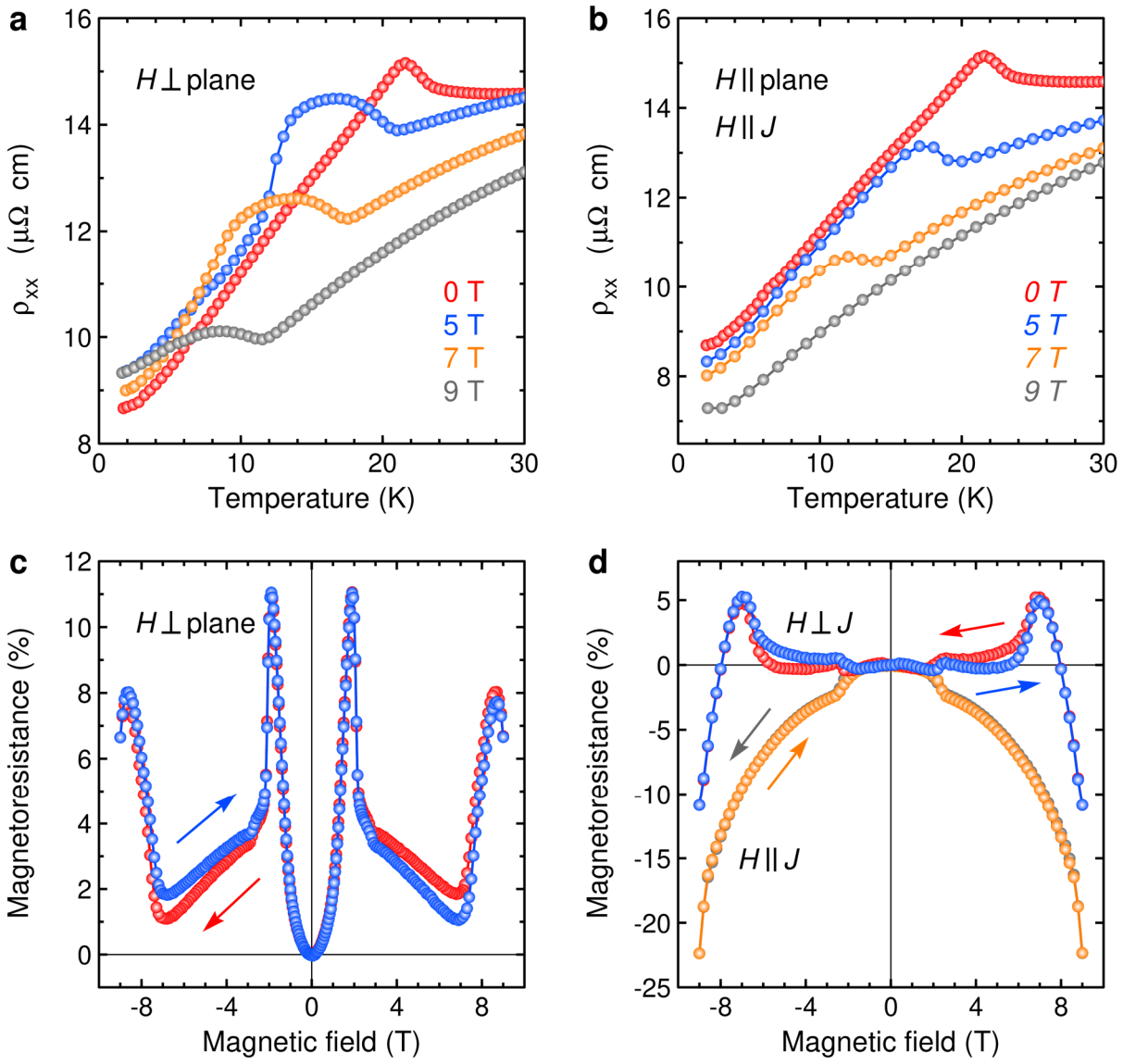

Fig. 4. Electron transport in $GdAl_2Ge_2$ (d = 38 nm). a) Temperature dependence of resistivity in out-of-plane magnetic fields 0 T (red), 5 T (blue), 7 T (orange), and 9 T (grey). b) Temperature dependence of resistivity in in-plane magnetic fields 0 T (red), 5 T (blue), 7 T (orange), and 9 T (grey) parallel to the current J. c) Hysteretic behaviour of MR at T = 2 K in out-of-plane magnetic fields. d) Hysteretic behaviour of MR at T = 2 K in in-plane magnetic fields parallel (grey and orange) and perpendicular (red and blue) to the current J.

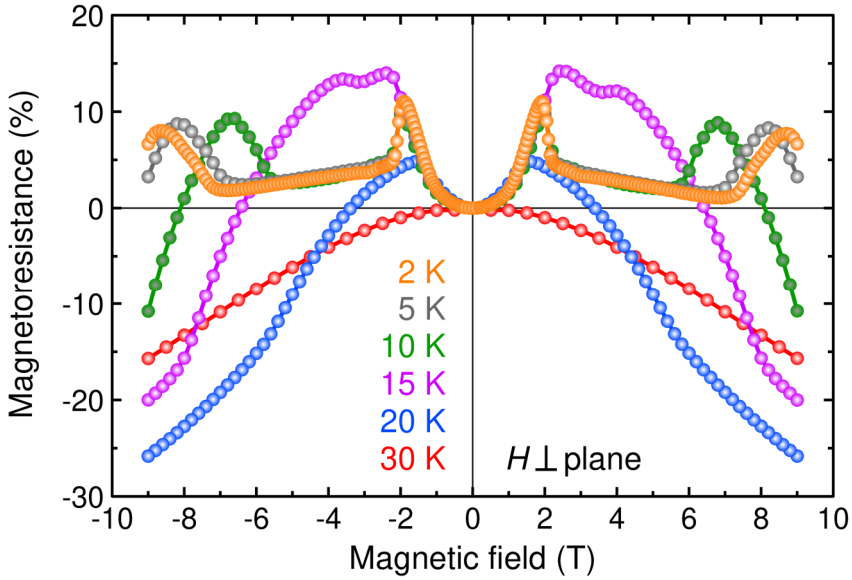

Fig. 5. MR in $GdAl_2Ge_2$ (d = 38 nm) for out-of-plane magnetic fields at 2 K (orange), 5 K (grey), 10 K (green), 15 K (magenta), 20 K (blue), and 30 K (red).